The Magnetic O star θ^1 Orionis C

θ^1 Ori C (O7 V) is the ionizing source of the Orion Nebula and a source of hard, variable X-ray emission, with its X-ray flux modulated on the star's 15.4-day rotation period (Gagné, et al. 1997, ApJ, 482, 569). Figure 1 shows an 850 ks *Chandra* image of the Orion Nebula. Although θ^1 Ori C is severely piled up at the ACIS-I aimpoint, the light curve was extracted from the wings of the PSF. The data points in the right panel of Fig. 1 show the visible emission measure decreasing by $\sim 30\%$ from X-ray maximum to minimum as part of the X-ray emitting torus passes behind the photosphere. The X-ray dip coincides with a dip in the Hα emission (i.e., as an increase in the Hα equivalent width).

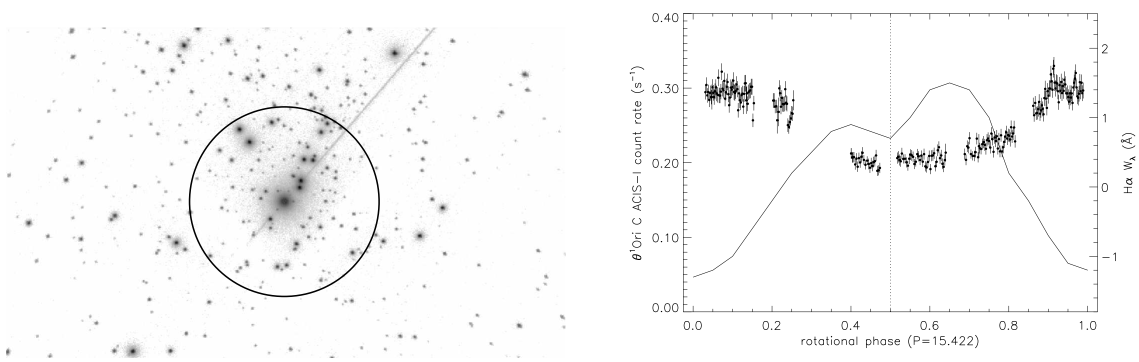

Fig. 1.— *Left: Chandra* Ultra-Deep field centered on θ^1 Ori C. The central star emits $\approx 75\%$ of the flux at Fe Kα within the $1'$ XRS XRT half-power radius (black circle). *Right:* θ^1 Ori C ACIS-I light curve spanning most of the 15.422-day rotation period. The XRS observations would occur near phases 0.0 and 0.5 (viewing angles 3° and 87°). The solid line shows the Hα equivalent width variations (right axis).

To date, θ^1 Ori C is the only O star with a measured magnetic field: Donati, et al. (2002, MNRAS, 333, 55) detect a dipole field strength $B \approx 1100$ G. The rotationally-modulated longitudinal magnetic field suggests an oblique magnetic rotator whose magnetic dipole axis is tilted to the rotation axis by about 42°. The 45° tilt of the rotation axis to our line of sight produces the large-amplitude variability seen in X-rays, optical emission lines (Stahl, et al. 1996, A&A, 312, 539) and UV C IV and Si IV P-Cygni profiles (Walborn & Nichols 1994, ApJ, 425, L29).

θ^1 Ori C appears to be the prototype of a new class of X-ray source: a young, hot star with a strong, large-scale magnetic field. Building on the magnetic geometry of Bp stars suggested by Shore & Brown (1990, ApJ, 365, 665), Babel & Montmerle (1997, ApJ, 485, L29) proposed the magnetically confined wind-shock (MCWS) mechanism for θ^1 Ori C, whereby the star's radiation-driven wind is channeled along magnetic field lines, leading to strong, X-ray emitting shocks, formed at the magnetic equator by the collision of wind streams from opposing hemispheres.

The Magnetically Channeled Wind Shock Model

Expanding on the MCWS model, ud-Doula & Owocki (2002, ApJ, 576, 413) performed isothermal 2-D MHD simulations to show that for all but the strongest fields, the field geometry is strongly affected by the wind kinetic energy and most previously-closed field lines are ripped open, with an associated reduction in the magnetic field's ability to focus the flow. Even in the strong-field case, there are regions of the wind where the field lines are not closed (generally near the magnetic poles and in the equatorial plane far away from the photosphere).

Our latest 2D simulations for θ^1 Ori C include adiabatic and radiative cooling as well as shock heating in the MHD code's energy equation. In this way, we make quantitative predictions of plasma temperature and X-ray emission. Figure 2 is a snapshot of temperature/density (squared) and the resulting field distortion. In this snapshot, the bulk of the X-rays are emitted in the hottest plasma with the highest emission measure, close to the last closed magnetic contour. At other times (not shown), the shock-heated plasma fills closed field regions, grows in density until it can no longer be supported by magnetic tension against the inward pull of gravity, and falls back down onto the photosphere along field lines above or below the magnetic equator. The MHD simulations make three important predictions: (1) wind shocks produce plasma up to $\log T \approx 7.6$, (2) most of the X-rays are produced at a radius $1.4 - 2.4R_\star$, (3) the flow produces a dense cooling disk from $1 - 2R_\star$.

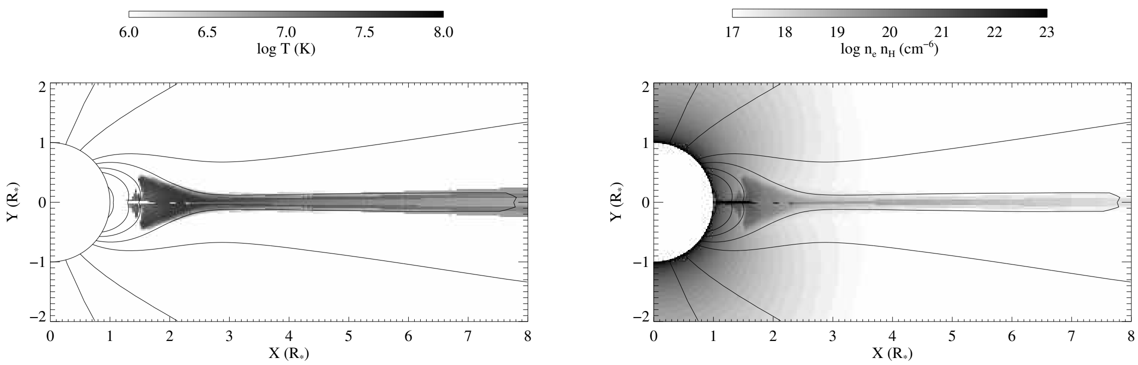

Fig. 2.— 2D MHD simulation of magnetically channeled wind shocks on θ^1 Ori C. The rotation axis is inclined 45° to the vertical magnetic axis. X-ray maximum occurs when the star is viewed magnetic pole-on, i.e., from above or below. X-ray minimum occurs when the star is viewed equator-on, i.e., from the left. Magnetic field lines (solid contours) are plotted over grayscale images of $\log T$ (left) and $\log n_e n_H$ (right). Most of the X-rays are produced around $R \approx 1.8R_\star$. The cooling disk is visible in the magnetic equatorial plane.

Chandra HETG Results

Chandra obtained HETG spectra at four rotational phases of θ^1 Ori C, confirming many of the predictions of the MCWS model (Gagné et al. 2004, ApJ, submitted, astro-ph). The spectrum shows a strong 2-10 Å continuum and bright Ne X, Mg XII, Si XIII, Si XIV, S XV, S XVI, Ar XVII, Ca XIX, and Fe XXV lines. Spectral fits indicate an approximately solar-abundance 2T VAPEC plasma with a dominant temperature of $T \approx 30$ MK.

Our line-profile analysis of the HEG/MEG spectra finds small but significant non-thermal line broadening of ≈ 300 km s^{-1} in most lines. There is also a hint that the lines may be redshifted when the disk is viewed edge-on (at large viewing angles). The line widths may be the result of turbulent flows in the post-shock plasma, while the line shifts may be direct evidence of infalling material.

Kahn et al. (2001, A&A, 365, L312), recalling the early work of Gabriel & Jordan (1969, MNRAS, 145, 241), pointed out that high-resolution X-ray spectra of O-type stars can be used to probe the location of the

X-ray emitting plasma. Electrons in the $^3\mathrm{S}_1$ state of He-like ions can be photoexcited by photospheric UV radiation to the $^3\mathrm{P}$ states, thereby suppressing the $^3\mathrm{S}_1 \rightarrow {}^1\mathrm{S}_0$ forbidden line and enhancing the $^3\mathrm{P}_{1,2} \rightarrow {}^1\mathrm{S}_0$ intercombination doublet. For low-Z ions like O VII, Ne IX and Mg XI, the FUV flux has been measured (or can be estimated from detailed model atmospheres). The ratio of the forbidden-to-intercombination line flux (f/i ratio) can then be used to measure the average distance between the X-ray emitter and the photosphere.

On θ^1 Ori C, the f/i ratios of Mg XI, Si XIII, and S XV suggest those X-rays are produced at a radius of $1.2 - 1.8R_\star$, consistent with the observed eclipse fraction. At these high temperatures, the dielectronic recombination satellite (DES) lines of S XV, Ca XIX and Fe XXV are sensitive temperature diagnostics (Oelgoetz & Pradhan 2004, MNRAS, in press, astro-ph/0408065). DES lines were not resolved with *Chandra*. Similarly, H-like Fe XXVI lines, formed only in very hot ($T > 50$ MK) plasma, were not detected. Higher throughput and higher spectral resolution at S XV (2.45 keV), Ca XIX (3.89 keV), Fe XXV (6.69 keV) and Fe XXVI (6.90 keV) are needed to more accurately measure the temperature and location of the hottest plasma.

One important prediction of the MCWS model is the formation of a cool, dense disk from $1 - 2R_\star$ as shocked plasma in the magnetic equatoral plane radiatively cools and falls back onto the photosphere. Some of the hard X-rays should be reprocessed by the disk, producing Fe Kα fluorescent line emission. The strength of the Fe Kα fluorescence line depends on the column density of the disk, the geometry of the system, and the incident hard X-ray flux. The Fe Kα feature at 6.4 keV is routinely detected on X-ray binaries and AGN and was seen on the B0.5e star γ Cassiopeiae (Smith, Cohen, Gu, Robinson, Evans, & Schran, 2004, ApJ, 600, 972). The 6.4 keV line was not detected on θ^1 Ori C with *Chandra*, though the 3σ upper limit $W_\lambda > -85$ mA is much brighter than the -20 mA detection on γ Cas.

Astro-E2 XRS Spectra of θ^1 Ori C

The unsurpassed effective area and spectral resolution of the XRS beyond 2 keV will allow us to measure five key diagnostics at orthogonal viewing angles of θ^1 Ori C: (1) fluorescent Fe Kα to probe the density and location of the cooling disk, (2) S XV, Ca XIX and Fe XXV f/i ratios, (3) S XV, Ca XIX and Fe XXV dielectronic satellite lines, (4) Fe XXV line profiles to measure line shifts and non-thermal line widths, and (5) Fe XXVI resonance lines to detect the hottest plasma.

Two 50 ks observations at opposite rotational phases are needed to look for viewing-angle dependent line shifts and column density. Using mulitple emission lines, a 50 ks XRS spectrum of θ^1 Ori C will detect $5 - 10$ km s^{-1} line shifts. In addition, the 0.5-10 keV XRS spectrum will be fit to provide tighter constraints on line width and abundance.

Because the He-like lines are sensitive to temperature, abundance, density, and EUV/FUV radiation (see, e.g., Gabriel & Jordan 1969), the line complexes in Figure 3 have been modeled using the PrismSPECT non-LTE excitation kinematics code (MacFarlane et al. 2003, Proceedings of the 3rd International Conference on Inertial Fusion Sciences and Applications, Amer. Nucl. Soc.). For each line complex, we set up a model atom with several dozen levels for each ion using f-values and transition rates custom-computed using Hartree-Fock and distorted wave methodologies. The resulting values are checked against data from the literature. We include collisional and radiative coupling among most levels in the model atom, and specifically include photoexcitation between the $^3\mathrm{S}_1$ and $^3\mathrm{P}_{1,2}$ levels driven by photospheric radiation.

Fig. 3 (left panel) demonstrates the diagnostic potential of the XRS at S XV. The PrismSPECT XRS simulation at left assumes a 30 MK plasma in a $R = 1.8R_\star$ torus (the *Chandra* 1σ lower limit) around a 45000 K photosphere. In Fig. 3 (right panel), a 300 km s^{-1}-wide Gaussian line at 6.4 keV with $W_\lambda = -85$ mA has been added to illustrate Fe Kα fluorescence. Our 100 ks total exposure time request has been chosen to achieve a limiting detection threshold $W_\lambda = -20$ mA. The PrismSPECT simulation shows that the Fe XXV forbidden (z), DES, intercombination (x, y) and resonance (w) lines will be fully resolved with the XRS.

The $^3S_1 \rightarrow {}^3P_{1,2}$ excitations of He-like Fe, Ca, Ar, S and Si occur in the EUV, shortward of the Lyman limit, from $271-865$ Å. Because this portion of the EUV is completely absorbed by interstellar gas, synthetic spectra are needed. Unfortunately, the line lists used by Hubeny & Lanz (1995, ApJ, 439, 875) and others to compute non-LTE model atmospheres and spectra cutoff at 880 Å. To accurately model the He-like line complexes observed with the XRS, we propose to compute TLUSTY model atmospheres and SYNSPEC synthetic spectra for θ^1 Ori C with line lists containing all available transitions from $200-2000$ Å.

As is evident in the left panel of Fig. 1, the XRS blur circle will contain emission from ≈ 100 known X-ray sources. We estimate that $\approx 75\%$ of the $2-10$ keV flux on the central XRS diodes will be emitted by θ^1 Ori C. To achieve our science goals, we plan to use Orion Ultra-Deep Field images and spectra as input to XRSSIM to account for emission from the other sources on each XRS diode. Although many of the Trapezium stars exhibit X-ray flares, they are individually $10^1 - 10^4$ times fainter than θ^1 Ori C. As a result we are confident we can account for their time-averaged emission, although this will lead to some predictable systematic errors.

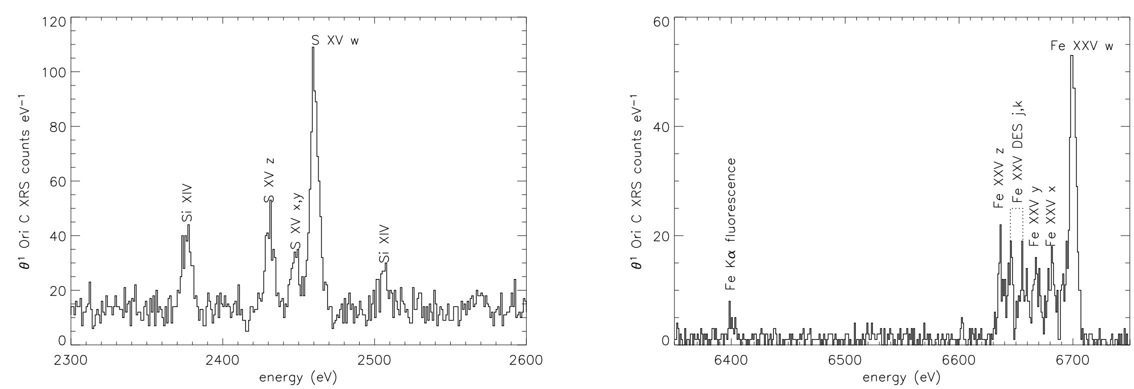

Fig. 3.— *Left:* Simulated 100 ks XRS spectrum of θ^1 Ori C showing the He-like S XV complex near 2.45 keV. *Right:* the XRS FeXXV resonance (w), intercombination (x,y), forbidden (z), and dielectronic recombination satellite (j,k) lines and the Kα Fe fluorescence from the cooler disk. Note that the Fe XXV intercombination lines are well resolved with XRS.

XIS Imaging Spectroscopy of the Trapezium Cluster

The XIS field of view will contain over 2000 X-ray sources as seen in the Orion Ultra-Deep Field. Approximately 900 sources outside the immediate vicinity of θ^1 Ori C will be detected and spatially resolved with XIS in 100 ks. Most of these sources are low-mass classical and weak-lined T Tauri stars with hard, time-variable X-ray spectra. The XIS will detect hundreds of X-ray flares on these stars; $30-50$ flares will be strong enough for detailed, time-resolved CCD spectroscopy (e.g., Gagné, Skinner, & Daniel 2004, ApJ, 613, in press, astro-ph/0405467).